Conservation of the direct and indirect pathways dichotomy in mouse caudal striatum with uneven distribution of dopamine receptor D1- and D2-expressing neurons

Kumiko Ogata[1], Fuko Kadono[2], Yasuharu Hirai[1,2], Ken-ichi Inoue[3], Masahiko Takada[3], Fuyuki Karube[1,2] † , and Fumino Fujiyama[1,2] †

[1]Laboratory of Neural Circuitry, Graduate School of Brain Science, Doshisha University, Kyotanabe 610-0394, Japan

[2]Laboratory of Histology and Cytology, Faculty of Medicine and Graduate School of Medicine, Hokkaido University, Sapporo 060-8638, Japan

[3]Systems Neuroscience Section, Primate Research Institute, Kyoto University, Inuyama, Aichi 484-8506, Japan

† These authors share senior and last authorship.

*** Correspondence:**
Prof. Fumino Fujiyama and Fuyuki Karube
fujiyama@pop.med.hokudai.ac.jp and karube@med.hokudai.ac.jp

Keywords: striatum; substantia nigra pars lateralis; dopamine receptor; tyrosine hydroxylase; basal ganglia; direct pathway; indirect pathway

Abstract

The striatum is one of the key nuclei for adequate control of voluntary behaviors and reinforcement learning. Two striatal projection neuron types, expressing either dopamine receptor D1 (D1R) or dopamine receptor D2 (D2R) constitute two independent output routes: the direct or indirect pathways, respectively. These pathways co-work in balance to achieve coordinated behavior. Two projection neuron types are equivalently intermingled in most striatal space. However, recent studies revealed two atypical zones in the caudal striatum: the zone in which D1R-neurons are the minor population (D1R-poor zone) and that in which D2R-neurons are the minority (D2R-poor zone). It remains obscure as to whether these imbalanced zones have similar properties on axonal projections and electrophysiology to other striatal regions. Based on morphological experiments in mice using immunofluorescence, *in situ* hybridization, and neural tracing, here, we revealed the poor zones densely projected to the globus pallidus and substantia nigra pars lateralis, with a few collaterals in substantia nigra pars reticulata and compacta. As other striatal regions, D1R-neurons were the direct pathway neurons, while projection neurons in the poor zones possessed similar electrophysiological membrane properties to those in the conventional striatum using *in vitro* electrophysiological recording. In addition, the poor zones existed irrespective of the age of mice. We also identified the poor zones in the common marmoset as well as other rodents. These results suggest that the poor zones in the caudal striatum follow the conventional projection patterns irrespective of imbalanced distribution of projection neurons. The poor zones could be an innate structure and common in mammals and relate to specific functions via highly restricted projections.

1 Introduction

The striatum regulates voluntary movement and reward-related learning by integrating excitatory inputs from the cerebral cortex and thalamus (Alexander et al., 1986; Hikosaka et al., 2000; Kreitzer and Malenka, 2008; Peak et al., 2019; Redgrave et al., 2011). The medium spiny projection neurons (MSNs), the major population of striatal neurons, are classified into two groups, direct and indirect pathway neurons, depending on their projection targets and gene expression. The direct pathway MSNs (dMSNs) transmit information to output nuclei, such as entopeduncular nucleus (EP) and substantia nigra (SN), directly. The dMSNs express GABA, dopamine receptor D1 (D1R), and substance P. In contrast, indirect pathway MSNs express GABA, dopamine receptor D2 (D2R), and enkephalin and indirectly project to the output nuclei via the globus pallidus (GP) and subthalamic nucleus (Albin et al., 1989; Alexander and Crutcher 1990; Graybiel, 1990). It has long been believed that both types of projection neurons are randomly distributed (Gerfen, 1989; Lança et al., 1986; Tinterri et al., 2018), and each local striatal area contains an almost equal proportion of both types (Hedreen and DeLong, 1991; Selemon and Goldman-Rakic, 1990).

Dense and topographic corticostriatal innervation recruits striatal subregions for specific functions (Nambu, 2008; Shepherd, 2013; Shipp, 2016). The caudal striatum (cStr) in rodents lies under the temporal cortical area and is similar to the caudate tail (CDt) in primates, which is a curved long extension of the ventral part of the caudate nucleus. Temporal areas, including somatosensory, visual, and auditory related areas, innervate cStr in rodents (Deniau et al., 1996; Hintiryan et al., 2016; Hunnicutt et al., 2016; Jiang and Kim, 2018; Xiong et al., 2015) and CDt in primates (Brown et al., 1995; Caan et al., 1984; Saint-Cyr et al., 1990; Yeterian and Pandya, 1998; Yeterian and Van Hoesen, 1978); therefore, they are considered the sensory striatum. In addition, similar to cStr in rodents (Menegas et al., 2015; Watabe-Uchida et al., 2012), CDt in primates receives the projection from a specific group of dopaminergic neurons (Kim et al., 2014; Kim and Hikosaka, 2013). Thus, cStr in rodents and CDt in primates share common neural connection features. The functional significance of CDt and cStr has been also gradually uncovered. CDt in primates is involved in the distinct functions such as coding value of objects (Griggs et al., 2017; Kim et al., 2017; Kim et al., 2014; Kim and Hikosaka, 2013). Recent studies in rodents have shown that the cStr is involved in the avoidance behavior of mice (Menegas et al., 2018; Menegas et al., 2017).

Gangarossa et al. (2013) revealed a unique cStr region adjacent to GP using BAC transgenic mice that express eGFP. The region is surprisingly composed almost exclusively of *Drd1a* expressing neurons and is therefore called D2R/A2aR-expressing MSNs-poor zone (Gangarossa et al., 2013). Studies with transgenic mice showed the difference in the proportion of D1R and D2R-expressing neurons in the cStr (Miyamoto et al., 2018; Miyamoto et al., 2019; for review, see Valjent and Gangarossa, 2021). Our previous study with wild-type mice also confirmed the highly uneven distribution of D1R and D2R immunoreaction in the unique regions of cStr (Ogata et al., 2018).

Although such uneven distribution of D1R and D2R immunoreactivity conjures up the possibility that the direct and indirect pathway neurons are separately distributed in these regions of cStr, it contradicts the conservative model according to which the physiological function requires a balance of the direct and indirect pathway neurons mediated by D1R and D2R, respectively (Calabresi et al., 2014; Cui et al., 2013; Friend and Kravitz, 2014; Isomura et al., 2013). Thus, we raise two questions: First, does the uneven distribution of D1R and D2R immunoreactions actually reflect separate distribution of the direct and indirect pathway projection neurons? If so, what are neural

circuitries driven by? Second, is this uneven distribution a common property of the sensory related striatum and conserved among rodents and primates, or a rodent-specific feature (Gangarossa et al., 2019)? If the former, sensory inputs may modify the uneven structure of the sensory related striatum. Thus, the uneven structure may vary developmentally, since neonatal mice do not respond to visual and auditory stimuli (Huberman et al., 2008; Sonntag et al., 2009), while aged C57BL6 mice typically have impaired hearing (Zheng et al., 1999). Alternatively, the uneven structure of the cStr can be innate, although maturation of MSNs continues in the early postnatal days (Krajeski et al., 2019). To address these questions, we employed a combination of *in situ* hybridization, immunohistochemistry, electrophysiological recording, and retrograde/anterograde tracing in mice, and compared the cStr across ages and species.

2 Materials and Methods

All animal experiments in the mice and rats were approved and performed in accordance with the guidelines for the care and use of laboratory animals established by the Committee for Animal Care and Use of Doshisha University (Approval number: A16008, A17001, A18001, A19036, and A20057) and the Animal Care and Use Committee of Hokkaido University (Approval Number: 20-0106). All animal studies in the common marmoset were conducted in accordance with experimental procedure protocols approved by the Animal Welfare and Animal Care Committee of the Primate Research Institute of Kyoto University (Approval number: 2017-031). All efforts were made to minimize animal suffering and the number of animals used. Chemicals were purchased from Nacalai Tesque (Kyoto, Japan) and Wako (Osaka, Japan), unless otherwise noted.

In this study, 42-wild type C57BL/6J male mice (8-day-old–172-week-old), three wild type slc:ICR male mice (11 weeks old), three Long-Evans male rats (11−13 week old), three Wistar male rats (12-week-old), and two common marmosets (a 6-year-old male and a 5-year-old female) were used.

2.1 Animal surgery: Retro- and anterograde tracing study

Mice were anesthetized by inhalation of isoflurane (Pfizer Japan Inc., Tokyo, Japan) followed by intramuscular injection of a mixture of ketamine (Ketalar; Daiichi-Sankyo, Tokyo, Japan; 40 mg/kg) and xylazine (Bayer HealthCare, Tokyo, Japan; 4 mg/kg). Before and after surgery, butorphanol solution (Meiji Seika Pharma Co Ltd, Tokyo, Japan) was injected subcutaneously (0.2 mg/kg) for analgesia. Each mouse was then fixed to a stereotaxic device (Narishige, Tokyo, Japan). During surgery, the body temperature of the mice was monitored and maintained at approximately 38□ (BWT 100A animal warmer, Bio Research Center, Nagoya, Japan). The skull was drilled to make a small hole in an appropriate position in accordance with the mouse brain atlas (Paxinos and Franklin, 2013). For retrograde tracing combined with *in situ* hybridization, a large volume (> 0.5 µL) of 0.2% cholera toxin subunit B – Alexa Fluor 555 (CTB555) or 488 (CTB488) conjugate (C22843 or C-22841, Thermo fisher Scientific, Inc.) in 0.1 M phosphate buffer (PB, pH 7.4) was injected around the output nuclei of the basal ganglia of 3 mice [anteroposterior (AP): 2.8 mm caudal from the bregma (AP -2.8), lateromedial (LM): 2.1 mm lateral from the midline (L 2.1), depth: 3.7−4.2 mm from the pial surface (D 3.7−4.2)] using a glass pipette (tip diameter, 15−20 µm) through which air pressure pulses were delivered with a pressure injector (PV820, World Precision Instruments, Sarasota, FL, USA). The site of injection extended to the substantia nigra pars reticulata (SNr), substantia nigra pars compacta (SNpc), and entopeduncular nucleus (EP), but did not reach the GP. For retrograde tracing from substantia nigra pars lateralis (SNpl) or medial

geniculate nucleus (MG), 0.2% CTB555 (~0.2 µl) was injected by pressure, or 5% fluorogold (FG) solved in phosphate-buffered saline (PBS) was injected iontophoretically (0.8−1.0 µA positive current pulses with a 7 s-on/off cycle for 5 min using A365, World Precision Instruments). The coordinates of the injection were [AP -2.9, L 1.8, D 3.8] for SNpl and [AP -3.2, L 2.0, D 2.8] for MG (N = 3 mice for each).

For anterograde tracing, 10% biotinylated dextran amine (BDA; D1956, Invitrogen) in phosphate-buffered saline (PBS, pH 7.4) or 2.5% Phaseolus Vulgaris Leucoagglutinin (PHAL; L-1110, Vector laboratories) in 10 mM phosphate (pH 8.0) was injected in the cStr using a glass pipette (tip diameter, 15−25 µm). The BDA solution was injected iontophoretically by a 1.2 µA current pulses with a 7 s-on/off cycle for 5−20 min, or ejected by a single air pulse. PHAL was injected by 4 µA current pulses with a 7 s on/off cycle for 5 min. After 3−5 days, each mouse was perfused as described below. The targeted coordinates for cdStr were [AP -1.2, L 2.7, D 1.7], and those for D1R- and/or D2R-poor zones were [AP -1.2, L 2.7, D 2.8].

2.2 Immunofluorescence labeling and tracer visualization

2.2.1 Tissue preparation

Mice and rats were deeply anesthetized with isoflurane and sodium pentobarbital (100 mg/kg, i.p.; Kyoritsu Seiyaku Corporation, Tokyo, Japan). The animals were then transcardially perfused with 8.5% sucrose in 20 mM PB containing 5 mM $MgCl_2$, followed by 4% w/v paraformaldehyde and 75% saturated picric acid in 0.1 M PB. After perfusion pump off, the brain was postfixed *in situ* for 1.5 h at room temperature (RT; 25 ± 3□), and then the brain was removed from the skull followed by cryoprotection with 30% sucrose in PBS for 24−48h at 4□. Tissue blocks containing the striatum were sectioned sagittally or coronally using a freezing microtome (Leica Microsystems, Wetzlar, Germany) at a thickness of 20 µm. Six series of floating sections were collected in 0.1 M PB containing 0.02% of sodium azide and prepared for immunofluorescence labeling.

Two common marmosets (*Callithrix jacchus*; one male and one female) weighing around 370 g were used for this study. They were caged at 27 ± 2 °C in 50 ± 10% humidity with a 12-h light–dark cycle and were fed twice a day with a standard marmoset diet supplemented with fruit, mealworm, and gum with vitamin D. Water was available ad libitum. Following sedation with ketamine hydrochloride (40 mg/kg, i.m.), the marmosets were deeply anesthetized with an overdose of sodium pentobarbital (50 mg/kg, i.v.) for perfusion-fixation. The marmosets were transcardially perfused with 0.1 M PBS (pH 7.4) followed by 4% paraformaldehyde in 0.1 M PB (pH 7.4). The brain was removed from the skull, postfixed in the same fresh fixative overnight, and saturated with 30% sucrose in PB at 4˚C. Tissue blocks containing the putamen and caudate nucleus were sectioned coronally using a freezing microtome at a thickness of 25 µm. Twelve series of floating sections were collected in 0.1 M PB containing 0.02% of sodium azide and prepared for immunofluorescence labeling.

2.2.2 Immunofluorescence labeling

The sections of mice, rats, and marmosets were incubated with a mixture of primary antibodies overnight at RT (Table 1). The primary antibodies were diluted with incubation buffer containing 10% (v/v) normal donkey serum (Merck KGaA, Darmstadt, Germany), 2% bovine serum albumin and 0.5% (v/v) Triton X-100 in 0.05 M Tris-buffered saline (TBS). After exposure to the primary antibodies, the sections were washed in TBS and incubated for 3 h at RT in the same buffer containing a mixture of secondary antibodies (Table 2). In some cases, the whole immunoreaction steps were repeated to enhance signals. After rinsing, the sections were mounted on to glass slides, air dried, and cover-slipped with 50% (v/v) glycerol/TBS.

2.2.3 Tracer visualization

BDA was visualized with fluorophore-conjugated streptavidin (Thermo Fisher Scientific; 1:1,000 for 3 h) combined with a tyramine signal amplification method. PHAL was detected using immunofluorescence.

2.3 *In situ* hybridization and NeuN immunolabeling

All *in situ* hybridization experiments were accomplished under a ribonuclease-free condition. Mice (C57BL/6J) for *in situ* hybridization were treated as above, except for exclusion of picric acid from the fixative. The following hybridization procedure was performed as reported previously (Hioki et al., 2010; Ma et al., 2011). Briefly, sagittal sections from both hemispheres were cut at 20 μm thickness using a freezing microtome. Free floating sections were hybridized for 16 − 20 h at 60□ with 1 μg/mL digoxigenin (DIG)-labeled sense or antisense riboprobes in a hybridization buffer. After washes and ribonuclease A (RNase A) treatment, the sections were incubated overnight with 1:1,000 diluted alkaline phosphatase-conjugated anti-DIG sheep antibody (11-093-274-910; Roche Diagnostics, Basel, Switzerland) and then reacted with 0.375 mg/mL nitroblue tetrazolium and 0.188 mg/mL 5-bromo-4-chloro-3-indolylphosphate (NBT/BCIP; Roche Diagnostics) for 27 − 42 hours. Sense probes detected no signal higher than the background. To sensitively detect the signals for Drd1a and Drd2 mRNA, we applied the biotinylated tyramine (BT)-glucose oxidase (GO) amplification method (Furuta et al., 2009; Ge et al., 2010; Kuramoto et al., 2009). Briefly, after hybridization with DIG-labeled Drd1a and Drd2 riboprobes, the sections were incubated with 1:4,000 diluted peroxidase-conjugated anti-DIG sheep antibody (11-207-733-910; Roche Diagnostics). Subsequently, the sections were reacted with a mixture containing 31 μM BT, 3 μg/mL of GO, 2 mg/mL of beta-D-glucose, and 2% bovine serum albumin in 0.1 M PB for 30 min. The sections were further incubated with 1:1,000 diluted alkaline phosphatase-conjugated streptavidin (02516-71; Nacalai Tesque) for 2 h and finally reacted with NBT/BCIP. The probes for Drd1a (target sequence position; 1116-1809 GenBank: NM_010076.3, Gifted from Shinichiro Okamoto) and for Drd2 (target sequence position; 1412-2497 GenBank: X55674.1, Gifted from Shinichiro Okamoto) were used.

After *in situ* hybridization, the sections were processed for NeuN immunohistochemistry with conventional visualization for bright microscopy using avidin-biotin-peroxidase complex (ABC Elite; Vector, Burlingame, CA) and diaminobenzidine. The stained sections were serially mounted onto the gelatinized glass slides, dried, washed in running water, dried again, cleared in xylene, and finally covered with mounting medium MX (Matsunami, Kishiwada, Japan) and a glass coverslip. The boundaries of the D1R- and D2R-poor zones were determined with double immunofluorescent staining for D1R and D2R using the adjacent section.

204

205

206 ## 2.4 Electrophysiological recording and post-hoc immunofluorescence

207 For *in vitro* slice recording, a mouse (postnatal 3–4 weeks) was deeply anesthetized with isoflurane
208 and decapitated. The brain was removed from the skull and immediately cooled for 2 min in ice-cold
209 artificial cerebrospinal fluid (ACSF) oxidized with 95% O_2/5% CO_2 gas. Then, a brain block
210 containing the striatum was resected and coronally sectioned into slices of 300 µm thickness using a
211 vibratome (7000smz-2, Campden, Leicestershire, UK) in cold ACSF. The sections were incubated
212 for 20 min at 32□ and then over 1 h at RT for recovery. Striatal neurons and neurons in the
213 neighboring nuclei were recorded using the whole cell patch clamp method with the aid of an EPC10
214 amplifier (HEKA Elektronik Dr. Schulze GmbH, Lambrecht/Pfalz, Germany). The pipette solution
215 was composed of K-gluconate 130; KCl_2; Na_2ATP 3; NaGTP 0.3; $MgCl_2$ 2; Na_4EGTA 0.6; HEPES
216 10; biocytin 20.1 (in mM). The pH was adjusted to 7.3 with KOH, and the osmolality was ~290
217 mOsm. After recording, the slices were fixed using fixative composed of 4% paraformaldehyde and
218 0.2% picric acid solved in 0.1 M PB overnight. The fixed slices were re-sectioned into 50 µm slices,
219 and the recorded neurons filled with biocytin were visualized using fluorophore-conjugated
220 streptavidin. The immunofluorescent reaction against DARPP32, known as a marker of MSNs, D1R,
221 and D2R was conducted as above to confirm the location of the recorded neurons and if they were
222 MSNs.

223

224 ## 2.5 Image acquisition and processing

225 The specimens were observed using microscopes (BZ-X710, Keyence, Osaka, Japan; BX53
226 equipped with a DP73 CCD camera, Olympus, Tokyo, Japan) or a confocal microscope (FV1200,
227 Olympus). For fluorescent imaging, appropriate filter sets (359–371-nm excitation and 397-nm
228 emission for Alexa Fluor (AF) 350 or 405; 450–490-nm excitation and 514–565-nm emission for
229 AF488; 530–585-nm excitation and 575–675-nm emission for AF594; 590–650-nm excitation and
230 655–675-nm emission for AF635) were applied. The images of each channel were obtained
231 sequentially and separately to negate possible crosstalk of signals across channels. Sections
232 processed for *in situ* hybridization were observed with bright field microscopy.

233 To quantify and compare immunofluorescent signals against D1R, D2R, and tyrosine hydroxylase
234 (TH) across the striatal regions and among individual mice, first D1R- and D2R-poor regions were
235 determined using line plots derived from corresponding images as shown in Figure 1B. The borders
236 between the rostral striatum and D1R-poor zone, D1R-poor zone and D2R-poor zone, or D2R-poor
237 zone and internal capsule, were determined using the derivative of each line plot as the point of
238 maximum slope. Then, the borders were used to obtain regions of interest (ROIs, 200 × 200 μm^2) in
239 each region. To measure pixel intensity of the ROIs, small areas containing nerve bundles were
240 masked.

241

2.6 Statistical comparison

All averaged values are represented as mean ± standard deviation. The quantitative values among groups (> 2) were compared using one-way ANOVA followed by the post-hoc Tukey test with the aid of commercial software: Microsoft Excel, R (language and environment for statistical computing and graphics similar to S, http://cran.r-project.org/), and MATLAB (MathWorks, Natick, MA). All p-values are presented. A p-value less than 0.05 is considered as statistically significant.

3 Results

3.1 Uneven distribution of immunoreactivity of D1R and D2R in the mouse caudal striatum

As compared with dorsal striatum (dStr), D1R-immunoreactivity was weak from 1.1 – 2.0 mm posterior to the bregma and from 2.8 mm to 3.3 mm lateral to the midline, whereas D2R-immunoreactivity was weak from 1.3 mm to 1.8 mm posterior to the bregma and from 2.7 mm to 3.2 mm lateral to the midline (L2.7 to L3.2) in mouse. An example sagittal section (L3.0) was shown in Figure 1A and 1B (see Supplementary Figure 1 for detailed spatial distribution). In the above range, expression of D1R, D2R, and TH was not uniform in the striatum, rather, the zone with weak D1R and that with weak D2R existed in the caudo-ventral portion of the striatum (arrowhead in Figure 1A; cf. Gangarossa et al., 2013; Miyamoto et al., 2019). Hereafter they are referred to as D1R-poor zone and D2R-poor zone, respectively. In these zones, immunofluorescence for TH was also weak (Figure 1A). This characteristic spatial expression of D1R, D2R, and TH was always observed in all samples used for this study (N = 42 mice). To quantify these changes of fluorescence, fluorescence intensity line plots were obtained for D1R, D2R, and TH as shown in Figure 1B (N = 3 mice). The fluorescent intensity was measured in ROIs located at the rostral striatum (rStr), D1R-poor zone, and D2R-poor zone, and then normalized by the values of rStr. Normalized D1R pixel intensity was significantly lower in D1R-poor zone (0.53 ± 0.02) than rStr (p = 0.00002) or D2R-poor zone (0.92 ± 0.06; p = 0.00008) by one-way ANOVA with post-hoc Tukey test. In contrast, D2R expression was significantly lower in D2R-poor zone (0.33 ± 0.08) than rStr (p = 0.00003) or D1R-poor zone (1.09 ± 0.03; p = 0,00001). TH pixel intensity was lower in D1R-poor zone and D2R-poor zone (0.41 ± 0.04 and 0.44 ± 0.03, respectively) than rStr (p = 0.000001 for D1R-poor zone and p = 0.000002 for D2R-poor zone).

Since TH expresses in adrenergic axons as well as dopaminergic axons, it does not directly indicate dopaminergic systems only. Dopamine transporter (DAT) is purely expressed in dopaminergic nervous system, thus, we examined whether DAT expression showed similar spatial pattern to TH. As shown in Supplementary Figure 2, DAT and TH is highly overlapped in the whole striatum, except for subcallosal zones where DAT expression was high. These results suggest that dopaminergic innervation in the cStr differs compared to the rStr.

3.2 Uneven distribution of mRNA of D1R and D2R in caudal striatal neurons in mice

Since D1R and D2R are also expressed in presynaptic terminals, it is not clear whether the above investigation reflects differential cellular composition of specific area of the cStr. Even if the fluorescence mainly came from cell bodies, different fluorescence intensity could reflect total neuronal density among striatal regions. To directly solve the question, we investigated mRNA

expression of Drd1a and Drd2 genes by *in situ* hybridization. A section containing the poor zones was used for *in situ* hybridization with NeuN immunostaining. To confirm the poor zone identity, the adjacent section was used for double immunofluorescent staining of D1R and D2R (Figure 2A, B, D, E). As shown in Figure 2, Drd1a (Figure 2A, B) and Drd2 (Figure 2D, E) were detected (dark blue) in cell bodies of striatal neurons expressing NeuN (brown). To compare zonal differences on the number and proportion of D1R- or D2R-neurons, we counted them in four areas using: rStr, para-poor zone, D1R-poor zone, and D2R-poor zone (see Figure 1A for subdivision of the striatum used in this study). The number of NeuN immunopositive cells did not significantly differ among four ROIs (N = 5,689 neurons in total from three mice, one section in each; $p = 0.14$; Figure 2G), suggesting that the cell density of the striatum, most of which probably regarded as the MSNs density, seems to be uniform even in the two poor-zones. The number of Drd1a or Drd2 expressing neurons were counted in one representative section for each mouse (N = 3 mice; N = 2,615 neurons for Drd1a and N = 3,074 neurons for Drd2). The proportion of Drd1a-expressing neurons to total neurons was 12.23 ± 1.43% (N = 73/593 neurons as sum of three mice) in D1R-poor zone, 82.06 ± 3.08% (N = 528/645) in D2R-poor zone, 50.44 ± 0.07% (N = 354/702) in rStr, and 46.49 ± 1.34% (N = 315/675) in para-poor zone, which were significantly different among these regions ($p = 0.0000507$ using one-way ANOVA). Post-hoc Tukey test revealed that the proportion of Drd1a-expressing neurons was significantly lower in D1R-poor zone ($p = 0.0000001$ *vs.* rStr; $p = 0.0000001$ *vs.* para-poor zone; $p = 0.0000001$ *vs.* D2R-poor zone), and significantly higher in D2R-poor zone than the other three regions ($p = 0.0000001$ *vs.* rStr; $p = 0.0000001$ vs para-poor zone) (Figure 2C). No significant difference was observed for rStr *vs.* para-poor zone ($p = 0.13$). On the other hand, the proportion of Drd2-expressing neurons to total neurons was 78.68 ± 1.73% (N = 539/686) in D1R-poor zone, 3.58 ± 1.19% (N = 28/786) in D2R-poor zone, 46.78 ± 4.23% (N = 366/781) in rStr, and 46.73 ± 4.13% (N = 382/821) in para-poor zone. The proportion was significantly different among these four regions ($p = 0.000006$ using one-way ANOVA). D2R-poor zone contained a significantly lower proportion of D2R-expressing neurons than the other regions ($p = 0.0000007$ *vs.* rStr; $p = 0.0000007$ *vs.* para-poor zone; $p = 0.0000001$ *vs.* D1R-poor zone). D1R-poor zone contained a significantly higher number of D2R-expressing neurons than others ($p = 0.0000076$ *vs.* rStr; $p = 0.0000075$ *vs.* para-poor zone) (Figure 2F). Again, no significant difference was observed between rStr and para-poor zone ($p = 0.99999$). Since we could not visualize both Drd1a and Drd2 simultaneously, composition of them in each area was elucidated as the sum of individual data in Figure 2H. These results clearly indicated distinct cell type composition of both D1R- and D2R-poor zones, in which either D2R or D1R expressing neurons occupied over 80% of total neurons.

3.3 MSNs in D1R- or D2R-poor zones possessed similar membrane properties to those in the dorsal striatum.

Since both poor zones are located close to the boundary between the striatum and the amygdala-striatal transition area (AST), we wondered whether these dopamine receptor poor zones are composed of MSNs possessing similar properties to other parts of the striatum. First, we confirmed DARPP32, a molecular marker of MSNs, expressed in 93.5 ± 0.9%, 92.6 ± 0.5%, and 92.1 ± 0.5% of NeuN-expressing cells in the dStr (N = 351 cells), D1R-poor zone (N = 374 cells), and D2R- poor zone (N = 469 cells), respectively (N = 3 mice). Second, whole cell patch clamp recordings were accomplished from medium sized neurons in those area, and recorded neurons were examined for

post-hoc immunofluorescence against DARPP32 (Figure 3). As a result, all medium sized neurons recorded in the dStr and D1R- or D2R-poor zone represented similar membrane properties, such as deep resting membrane potentials, narrow action potentials, and low input resistances ($p > 0.05$ by one-way-ANOVA; Figure 3C, Table 3). In addition, all neurons which possessed electrophysiological properties of MSNs expressed DARPP32 (N = 3 neurons in the dStr, N = 5 in D1R-poor zone, and N = 4 in D2R-poor zone). In some neurons, their dendrites were well visualized, and they were spiny (Figure 3B). Thus, both poor zones are composed of MSNs as the dStr is.

3.4 Retrogradely labeled direct pathway neurons were mainly distributed in D2R-poor zone in the mouse caudal striatum

To uncover whether D1R-expressing neurons in the poor zones project to the downstream basal ganglia nuclei as those in dStr, namely, direct pathway, retrograde neural tracing was conducted. Since the precise projection targets of the poor zones remain unknown, large volume of CTB555 or CTB488 was injected around wide brain regions located along with the striatonigral pathway. It is also important the injections must be located enough posterior to GP to avoid labeling of the indirect pathway neurons. As shown in Figure 4A, the tracer injection extended to the SNpr, SNpc, and EP, but not to GP which is the target of striatal indirect pathway neurons.

The retrogradely labeled neurons in the striatum appeared to be distributed in dStr and D2R-poor zone, avoiding D1R-poor zone (Figure 4B). For quantification, a ROI (512 × 512 pixels in images with resolution of 0.62 μm/pixel) was sampled from each striatal region as conducted for mRNA expression comparison written above: namely, dStr (Figure 4C1), para-poor zone (Figure 4C2), D1R-poor zone (Figure 4C3), and D2R-poor zone (Figure 4C4) from three mice (one section/mouse). In total, 2,252 retrogradely labeled neurons, which can be considered as direct pathway neurons, were counted stereologically. The density of labeled neurons in four striatal regions was significantly different ($p = 2 \times 10^{-6}$ using one-way ANOVA), and the density was lower in D1R-poor zone ($2.57 \pm 0.42 \times 10^4$ neurons/mm^3) than dStr ($7.52 \pm 0.50 \times 10^4$ neurons/mm^3, $p = 0.0018$ using post-hoc Tukey test), para-poor zone ($8.30 \pm 1.12 \times 10^4$ neurons/mm^3, $p = 0.00068$), or D2R-poor zone ($11.32 \pm 1.63 \times 10^4$ neurons/mm^3, $p = 0.00003$)(Figure 4D). In contrast, the density of labeled neurons in D2R-poor zone was significantly higher than dStr ($p = 0.009$) and D1R-poor zone, and para-poor zone ($p = 0.03$) (Figure 4D).

However, the relationship between dopamine receptor subtypes and projection properties, namely, direct pathway neurons express D1R wherein indirect pathway neurons express D2R, might not be applied to these atypical striatal regions. Thus, we also combined *in situ* hybridization with retrograde tracing study to examine D1R or D2R gene expression in retrogradely labeled neurons for bright field microscopy using immunoreaction against CTB. As shown in Figure 4E and F, CTB labeled neurons (brown), regarded as direct pathway neurons, expressed Drd1a (99.3%, N = 863/869) but not Drd2 (1.1%, N = 9/843) mRNA (blue).

3.5 Axonal projections from cdStr, D1R- or D2R-poor zones in mouse

So far, we showed D1R-poor zone is composed of ~80% of indirect pathway neurons expressing D2R and D2R-poor zone ~80% of direct pathway neurons expressing D1R. A crucial question to be

uncovered is whether outputs of D1R- and D2R-poor zones are similar to D1R- and D2R-neurons located in non-poor zones, the dorsal part of caudal striatum (cdStr; see Figure 1A for subdivision of the striatum used here). To visualize their axonal projections, small volume of anterograde tracer (BDA, 10 kD or PHAL) was injected to the cStr including D1R- and D2R-poor zones. Due to the small spatial volume of the poor zones, the deposit of BDA should be extremely small to avoid spreading BDA to neighboring striatal regions (Figure 5A). Using immunofluorescence against D1R and D2R, locations of injection sites were examined. As a result, we obtained four cases for injection to D1R-poor zone and one case for that to D2R-poor zone. In one remaining case, injection was centered at the border between D1R- and D2R-poor zones. For cdStr, the size of injection was larger than poor zones labeling (N = 3 mice). The resulted axon projection was similar in these injections. The labeled axons were mainly found in SNpl and GP (Figures 5 and 6), and probably they are targets of direct and indirect pathway MSNs, respectively. Notably, SNpl was a characteristic target of the direct pathway from the poor zones, whereas only a few collaterals were observed in EP, SNpr and SNpc (Figure 5, Supplementary Figure 3). We did not observe clear difference between projections from D1R- and D2R-poor zones, although only one sample was obtained for micro injection to D2R-poor zone. In comparison to the cdStr, poor zones tentatively projected to the dorsal part of SNpl whereas cdStr tended to project to the ventral part of SNpl. PHAL injection to cdStr labeled axons in EP and SNpr also, in addition to the SNpl. For projection to GP, the axons of both poor zones and cdStr were distributed in the caudal GP, not in the rostral GP (Figure 6A). Retrograde tracer injection to SNpl also labeled large neurons in the caudal GP, as well as putative MSNs in cStr including both D1R- and D2R-poor zones (Figure 6B).

We also observed the axons in zona incerta, thalamic ventral posterior nucleus (VPM and VPL), thalamic reticular nucleus (Rt), medial geniculate nucleus (MG). Since in the cStr including poor zones, several neural fibers are passing through, BDA could provide ectopic labeling other than the injection center through such fibers or terminals in the striatum. We found a few labeled neurons in multiple cortical areas, thalamus, and brainstem; thus, the above ectopic labeling may be contaminated with actual striatal projections.

To confirm projection from the poor zones, retrograde tracers, fluorogold (FG) or CTB555, was injected into either MG or SNpl (Supplementary figure 4). We found prominent retrograde labeling in cStr by SNpl injection, as well as labeling in the caudal GP. Meanwhile, little to no labeling in cStr was observed by MG injection, and rather MG injection provided intensive labeling in the multiple cortical areas (the primary and secondary somatosensory area (S1 and S2); dorsal and ventral auditory area (Au), temporal association area (TEA) and amygdala. Thus, the main target of the direct pathway in the poor zones must be SNpl.

3.6 Uneven distribution of immunoreactivity of D1R and D2R in the caudal striatum across the age and species

To determine whether the uneven distribution of immunoreactivity of D1R and D2R in cStr is conserved across strains, C57BL/6J and ICR mice, and Long-Evans and Wistar rats were used for triple immunofluorescence of D1R, D2R and TH (N = 3 animals for each). In addition, to investigate

this uneven distribution is conserved across ages, young (postnatal 8 days, and 3-4 weeks) and old (60-172 weeks) C57BL/6J mice were also used for the triple immunofluorescence study (Figure 7).

In three young C57BL/6J mice (4-weeks old in Figure 7) examined, the uneven distribution of D1R, D2R, and TH was observed, with essentially the same spatial pattern as observed in adult mice (8-14 weeks). In addition, D1R- and D2R-poor zones still existed in old aged C57BL/6J mice (61 weeks, 111 weeks, and 172 weeks). The uneven distribution was also observed in ICR mice (11 weeks; N = 3). The uneven distribution of D1R and D2R were also found in the cStr of Wistar (N = 3, Figure 7C) and Long-Evans rats (N = 3, Figure 7D), as reported previously (Gangarossa et al., 2019). As the same as mice, D2R-poor zone was always located at the most caudal part of the striatum, and D1R-poor zone was rostral to and medial to D2R-poor zone, although the appearance (shape and size) was bit different from those in mice. The boundary of D1R- and D2R-poor zones extended to more dorsal in Long-Evans rats than Wister rats (Figure 7C and D).

To determine whether the uneven distribution of D1R, D2R, and TH is specific to rodents, the striatum of common marmosets, which is a nonhuman primate, was also examined (N = 2, Figure 7E, F). In the primate, the striatum exclusively subdivides further into two nuclei, the putamen and caudate nucleus. In the marmoset, the unique region with uneven distribution of D1R and D2R was found around the ventral tip of tail of the caudate (CDt). D1R- and D2R-poor zones adjoined, and D1R-poor zone was located laterally to D2R-poor zone, as observed in rodents. However, it is difficult to determine whether the spatial composition is similar to rodents due to anatomical structural differences of the striatum between them.

4 Discussion

In the present study, we demonstrated that in cStr, the rule of cellular correlation between dopamine receptor expression and projection pathways was conserved in the unusual part of the striatum where D1R-MSNs and D2R-MSNs are unevenly distributed. To the best of our knowledge, this is the first report which describes axonal projections from D1R-poor zones, although for D2R poor zone, Gangarossa et al. (2013) reported that it projected to SNpr and EP (Valjent & Gangarossa, 2020). We identified the characteristic projections from the poor zones to SNpl via the direct pathway, and to the caudal GP via the indirect pathway (Figures 5 and 6). We also showed that the electrophysiological properties of MSNs in the poor zones were similar to those observed in other striatal area (Figures 3, Table 3), and identified the poor zones in primates (Figure 7).

4.1 Methodological consideration

One may consider the present axonal tracing might be limited, since the tracer deposit in the poor zones must be extremely small. It could cause incomplete labeling. Therefore, we cannot exclude the possibility of additional projections to other brain areas not detected in the present study, and of potential projection differences from two poor zones. However, we also obtained the same results of axon labeling using adenoassociated viral vectors (AAV), which can increase sensitivity of visualization (data not shown). Moreover, the projections originated from a smaller population of MSNs in each poor zone, namely, D1R-neurons in D1R-poor zone or D2R-neurons in D2R-poor

zone, were successfully visualized. Thus, it is highly likely that characteristics of principal projections from the poor zones were obtained.

4.2 Dual pathway neurons in D1R- and D2R-poor zones

In transgenic mice, the uneven distribution of D1R and D2R expressing neurons in the cStr (Gangarossa et al., 2013, 2019; Miyamoto et al., 2019). The present study with wild type C57BL/6J mice also showed the uneven distribution of D1R and D2R expressing neurons in cStr and the coordinates of the boundary of D1R- and D2R-poor zones appear to be coincidence (Figures 1A-C).

The cellular distribution is not always the same as the distribution of immunoreactivity because the protein, which is visualized by immunohistochemistry, is expressed at not only soma but also dendrites and axons. We then performed *in situ* hybridization study and revealed the complementary distribution of Drd1a and Drd2 expressing neurons in both D1R- and D2R-poor zones (Figure 2H). These findings suggest the possibility that the direct and indirect pathway neurons are unevenly distributed in the cStr.

To address this question, we initially performed a retrograde tracing study combined with immunohistochemistry. The proportion of retrogradely labeled striatonigral neurons, considered as direct pathway neurons, were significantly lower in D1R-poor zone and significantly higher in D2R-poor zone than other regions (Figure 4A-D). It is noteworthy that the estimated density of striatal neurons by our large volume tracer injections is consistent with an early report (Rosen & Williams, 2001), suggesting that a large population of direct pathway neurons could be labeled and the differences on the labeled neuron density are not caused by biased topographic distribution of projection neurons. In addition, the combined study of *in situ* hybridization with retrogradely labeling showed that the retrogradely labeled direct pathway neurons expressed Drd1a, but not Drd2 mRNA (Figure 2E, F). These findings indicated that the distribution of direct pathway neurons in the cStr is highly biased toward D2R-poor zone. Owing to the existence of axon collaterals of the direct pathway neurons in GP (Fujiyama et al., 2011; Kawaguchi et al., 1990; Levesque and Parent, 2005), it is difficult to label only indirect pathway neurons using neural tracers. Nevertheless, our data suggested that D2R-neurons in the poor zones are likely to target GP as those in other striatal area, because the D1R-poor zone projection was denser in GP than in EP and/or SN (Figures 4 and 5). In addition, retrograde tracer injection revealed that both caudal GP and cStr convergently projected to SNpl. Thus, the direct and indirect pathway neurons in the poor zones could form complementary circuitry, even though they were distributed unevenly.

In addition, we showed the existence of D1R- and D2R-poor zones using young and aged C57BL/6J mice, ICR mice, Wister rats, Long-Evans rats, and common marmosets (Figure 7). The preservation of D1R- and D2R-poor zones across age and species suggest that such unique regions are necessary for information processing. The cStr, including poor zones, is innervated by the sensory cortices and suggests a possible relationship between sensory inputs and the poor zone development. However, it might be not the case. The poor zones were already present at ~P8, when behavioral reactions to tones or to visions are not yet elicited (Ehret, 1976; Huberman et al., 2008). Moreover the poor zones were preserved in aged C57BL6/J mice irrespective of their hard of hearing in general (Zheng

et al., 1999), although sensory deprivation affects synaptic transmission in the sensory striatum (Mowery et al., 2017). Thus, structure of the poor zones could develop and maintain without sensory signals.

4.3 The caudal striatum and the poor zone in rodents and primate

Recent studies with primate and rodent throw light on the functional aspect of the cStr. In the macaque monkey, the CDt, which is a long C-shaped structure of the ventral part of the caudate nucleus, has been reportedly involved in the distinct value function (Griggs et al., 2017; Kim et al., 2017; Kim et al., 2014; Kim and Hikosaka, 2013, 2015). These findings can also be explained by the CDt receiving the distinct subpopulation of dopaminergic neurons in SNpc. Meanwhile, the poor zones in the common marmosets revealed here were located in approximately the most rostral end of the CDt. This part of the CDt is small, therefore, its neural connection and function are still not clear. On the other hand, Menegas et al. (2017, 2018) reported that the tail of the striatum in rodents involved in the saliency and aversion. In addition, the shape of the poor zones also differed even in mice and rats (Figure 7). Thus, anatomical and functional similarity of the poor zones and the tail of the striatum among species warrants further research.

4.4 Functional implications of the poor zone

We reported that the main projection target of the cStr, including the poor zones, was SNpl. The previous studies reported that cStr subregions receiving auditory cortical inputs project to the SNpl, whereas cStr subregions receiving visual cortical inputs to the lateroventral SNpr (Deniau et al., 1996; Kohno et al., 1984). Such meso-scale topographic relationship was also reported in primates (Hedreen and DeLong, 1991). In turn, ventral SNpl is known to project to the superior colliculus (SC), inferior colliculus (IC), VPM, and so on; namely, it innervates the sensory-related regions of the thalamus and midbrain (Cebrian et al., 2005; Moriizumi et al., 1992; Takada, 1992; Yasui et al., 1991). In addition, cStr is innervated by sensory related cortical areas :auditory, visual, secondary sensory, TeA, and perirhinal areas(Hintiryan et al., 2016; Hunnicutt et al., 2016; Jiang and Kim, 2018; Yeterian and Pandya, 1998; Yeterian and Van Hoesen, 1978). Taken together, cStr can contribute to the gating and integration of multimodalities of sensation via SN in rodents, being similar to SN-subregion dependent information coding reported in primates (Amita et al., 2020; Kim and Hikosaka, 2015; Yamamoto et al., 2012; Yasuda and Hikosaka, 2015). Our anterograde and retrograde tracing also suggested that the caudal GP is likely to constitute the indirect pathway of cStr including poor zones, which projected to SNpl (Figure 6), as reported in primates (Amita and Hikosaka, 2019). Furthermore, cdStr and poor zones tended to project different parts of the SNpl (Supplementary Figure 3), which suggests a potential functional differentiation between cdStr and the poor zones.

4.5 Is the poor zone an exception of the striatum?

The classical model for the basal ganglia network suggests that normal function requires a balance of the direct and indirect pathway neurons mediated by D1R and D2R, respectively. The uneven distribution of the two MSNs population in the cStr raised a question regarding the balance between the direct and indirect pathway neurons. If the balance in the poor zones was as critical as other striatal areas, the two poor zones would share neural information with the aid of common inputs and/or mutual connections, or local circuitry within each zone. Whether D1R- and D2R-poor zones

share common cortical inputs remains to be determined; if they do, therefore two poor zones can work as one unit, like other striatal area containing equal number of D1R- and D2R-neurons. It is also possible that both poor zones could be innervated by different population of cortical neurons. In other striatal regions, the cortical axons in the adjoining striatal areas are originated from the adjacent but segregated cortical regions (Ghosh and Zador, 2021; Hooks et al., 2018). In such a case, two poor zones might communicate to compensate for the highly biased distribution of the direct and indirect pathway neurons, if they still need to work in a coordinated manner.

Alternatively, unlike motor or limbic related information processing in the striatum, these poor zones could work via either the direct or indirect pathway. If this was the case, lesser dopaminergic innervation specifically observed in the poor zones, which is likely to be from the SNpl (Jiang and Kim, 2018; Menegas et al., 2015; Poulin et al., 2018; Watabe-Uchida et al., 2012) could also relate to such unusual striatal circuitry. Furthermore, to determine whether the poor zones and cdStr are functionally differentiated, and whether the cStr is a counterpart of the primate CDt, neural tracing and functional recording/imaging in extremely fine scales are required, which will help to understand the two pathways beyond the current concept .

Abbreviations

ACSF, artificial cerebrospinal fluid; AP, antero-posterior; AST, amygdala-striatal transition area; Au, auditory area; BDA, biotinylated dextran amine; CDt, caudate tail; cStr, caudal striatum; cdStr, caudo-dorsal striatum; CTB, cholera toxin subunit B; DAT, dopamine transporter; dStr, dorsal striatum; D1R, dopamine receptor D1; D2R, dopamine receptor D2; EP, entopeduncular nucleus; FG, fluorogold; GP, globus pallidus; LM, latero-medial; MG, medial geniculate nucleus; MSN, medium spiny neuron; PB, phosphate buffer; PBS, phosphate buffered saline; PHAL, phaseolus vulgaris leucoagglutinin; ppz, para-poor zone; rStr, rostral striatum; RT, room temperature; SNpc, substantia nigra pars compacta; SNpl, substantia nigra pars lateralis; SNpr, substantia nigra par reticulata; TH, tyrosine hydroxylase; VPM, ventral posterior nucleus of thalamus, the medial part; VPL, ventral posterior nucleus of thalamus, the lateral part

5 Conflict of Interest

The authors declare that the research was conducted in the absence of any commercial or financial relationships that could be construed as a potential conflict of interest.

6 Author Contributions

All authors had full access to the data in the study and take responsibility for the integrity of the data and the accuracy of the data analysis. Conceptualization, F.F. and F. Karube; Methodology, F. Karube., Y.H. and K.O; Investigation, K.O., F. Karube, F. Kadono, Y.H., and F.F.; Formal Analysis, K.O., F. Kadono, F. Karube, and Y.H.; Resources, K.I. and M.T.; Writing - Original Draft, K.O., F.F. and F. Karube; Writing - Review & Editing, F.F. F. Karube, F. Kadono, K.O., Y.H; Visualization, K.O., F. Karube; Supervision, F.F. and F. Karube.; Funding Acquisition, F.F., F. Karube.

7 Funding

This study was funded by Grants-in-Aid from The Ministry of Education, Culture, Sports, Science, and Technology (MEXT) and Japan Society for the Promotion of Science (JSPS) for Scientific Research (20H03549 to FF) for Exploratory Research (20K20671 to FF) and for Scientific Researches on Innovative Areas “Hyper-Adaptability” (20H05484 to FF), and for Scientific Researches on Innovative Areas “Adaptation Circuit Census” (21H05241 to FF and to F. Karube).

8 Acknowledgments

We thank Drs. H Hioki and S Okamoto for suggestions on in situ hybridization. We thank Dr. S. Takahashi and Mr. T. Higashiyama for helpful discussion. We also thank Dr. Y Sakurai for supervision and kind encouragement.

9 References

Albin, R.L., Young, A.B., and Penney, J.B. (1989). The functional anatomy of basal ganglia disorders. Trends in neurosciences *12*, 366-375.

Alexander, G.E., and Crutcher , M.D. (1990). Functional architecture of basal ganglia circuits: neural substrates of parallel processing. . Trends in neurosciences *13*, 266–271.

Alexander, G.E., DeLong, M.R., and Strick, P.L. (1986). Parallel organization of functionally segregated circuits linking basal ganglia and cortex. Annual review of neuroscience *9*, 357-381.

Amita, H., and Hikosaka, O. (2019). Indirect pathway from caudate tail mediates rejection of bad objects in periphery. Sci Adv *5*, eaaw9297.

Amita, H., Kim, H.F., Inoue, K.I., Takada, M., and Hikosaka, O. (2020). Optogenetic manipulation of a value-coding pathway from the primate caudate tail facilitates saccadic gaze shift. Nature communications *11*, 1876.

Brown, V.J., Desimone, R., and Mishkin, M. (1995). Responses of cells in the tail of the caudate nucleus during visual discrimination learning. Journal of neurophysiology *74*, 1083-1094.

Caan, W., Perrett, D.I., and Rolls, E.T. (1984). Responses of striatal neurons in the behaving monkey. 2. Visual processing in the caudal neostriatum. Brain research *290*, 53-65.

Calabresi, P., Picconi, B., Tozzi, A., Ghiglieri, V., and Di Filippo, M. (2014). Direct and indirect pathways of basal ganglia: a critical reappraisal. Nature neuroscience *17*, 1022-1030.

Cebrian, C., Parent, A., and Prensa, L. (2005). Patterns of axonal branching of neurons of the substantia nigra pars reticulata and pars lateralis in the rat. The Journal of comparative neurology *492*, 349-369.

Cui, G., Jun, S.B., Jin, X., Pham, M.D., Vogel, S.S., Lovinger, D.M., and Costa, R.M. (2013). Concurrent activation of striatal direct and indirect pathways during action initiation. Nature *494*, 238-242.

Deniau, J.M., Menetrey, A., and Charpier, S. (1996). The lamellar organization of the rat substantia nigra pars reticulata: segregated patterns of striatal afferents and relationship to the topography of corticostriatal projections. Neuroscience *73*, 761-781.

Ehret, G. (1976). Development of absolute auditory thresholds in the house mouse (Mus musculus). J Am Audiol Soc *1*, 179-184.

Friend, D.M., and Kravitz, A.V. (2014). Working together: basal ganglia pathways in action selection. Trends in neurosciences *37*, 301-303.

Fujiyama, F., Sohn, J., Nakano, T., Furuta, T., Nakamura, K.C., Matsuda, W., and Kaneko, T. (2011). Exclusive and common targets of neostriatofugal projections of rat striosome neurons: a single neuron-tracing study using a viral vector. The European journal of neuroscience *33*, 668-677.

Furuta, T., Kaneko, T., and Deschenes, M. (2009). Septal neurons in barrel cortex derive their receptive field input from the lemniscal pathway. The Journal of neuroscience : the official journal of the Society for Neuroscience *29*, 4089-4095.

Gangarossa, G., Castell, L., Castro, L., Tarot, P., Veyrunes, F., Vincent, P., Bertaso, F., and Valjent, E. (2019). Contrasting patterns of ERK activation in the tail of the striatum in response to aversive and rewarding signals. Journal of neurochemistry *151*, 204-226.

Gangarossa, G., Espallergues, J., Mailly, P., De Bundel, D., de Kerchove d'Exaerde, A., Herve, D., Girault, J.A., Valjent, E., and Krieger, P. (2013). Spatial distribution of D1R- and D2R-expressing medium-sized spiny neurons differs along the rostro-caudal axis of the mouse dorsal striatum. Frontiers in neural circuits *7*, 124.

Ge, S.N., Ma, Y.F., Hioki, H., Wei, Y.Y., Kaneko, T., Mizuno, N., Gao, G.D., and Li, J.L. (2010). Coexpression of VGLUT1 and VGLUT2 in trigeminothalamic projection neurons in the principal sensory trigeminal nucleus of the rat. The Journal of comparative neurology *518*, 3149-3168.

Gerfen, C.R. (1989). The neostriatal mosaic: striatal patch-matrix organization is related to cortical lamination. Science *246*, 385-388.

Ghosh, S., and Zador, A.M. (2021). Corticostriatal Plasticity Established by Initial Learning Persists after Behavioral Reversal. eNeuro *8*.

Graybiel, A.M. (1990). Neurotransmitters and neuromodulators in the basal ganglia. Trends in neurosciences *13*, 244-254.

Griggs, W.S., Kim, H.F., Ghazizadeh, A., Gabriela Costello, M., Wall, K.M., and Hikosaka, O. (2017). Flexible and Stable Value Coding Areas in Caudate Head and Tail Receive Anatomically Distinct Cortical and Subcortical Inputs. Frontiers in neuroanatomy *11*, 106.

Hedreen, J.C., and DeLong, M.R. (1991). Organization of striatopallidal, striatonigral, and nigrostriatal projections in the macaque. The Journal of comparative neurology *304*, 569-595.

Hikosaka, O., Takikawa, Y., and Kawagoe, R. (2000). Role of the basal ganglia in the control of purposive saccadic eye movements. Physiological reviews *80*, 953-978.

Hintiryan, H., Foster, N.N., Bowman, I., Bay, M., Song, M.Y., Gou, L., Yamashita, S., Bienkowski, M.S., Zingg, B., Zhu, M., *et al.* (2016). The mouse cortico-striatal projectome. Nature neuroscience *19*, 1100-1114.

Hioki, H., Nakamura, H., Ma, Y.F., Konno, M., Hayakawa, T., Nakamura, K.C., Fujiyama, F., and Kaneko, T. (2010). Vesicular glutamate transporter 3-expressing nonserotonergic projection neurons constitute a subregion in the rat midbrain raphe nuclei. The Journal of comparative neurology *518*, 668-686.

Hooks, B.M., Papale, A.E., Paletzki, R.F., Feroze, M.W., Eastwood, B.S., Couey, J.J., Winnubst, J., Chandrashekar, J., and Gerfen, C.R. (2018). Topographic precision in sensory and motor corticostriatal projections varies across cell type and cortical area. Nature communications *9*, 3549.

659 Huberman, A.D., Feller, M.B., and Chapman, B. (2008). Mechanisms underlying development of
660 visual maps and receptive fields. Annual review of neuroscience *31*, 479-509.
661 Hunnicutt, B.J., Jongbloets, B.C., Birdsong, W.T., Gertz, K.J., Zhong, H., and Mao, T. (2016). A
662 comprehensive excitatory input map of the striatum reveals novel functional organization. eLife *5*.
663 Isomura, Y., Takekawa, T., Harukuni, R., Handa, T., Aizawa, H., Takada, M., and Fukai, T. (2013).
664 Reward-modulated motor information in identified striatum neurons. The Journal of neuroscience :
665 the official journal of the Society for Neuroscience *33*, 10209-10220.
666 Jiang, H., and Kim, H.F. (2018). Anatomical Inputs From the Sensory and Value Structures to the
667 Tail of the Rat Striatum. Frontiers in neuroanatomy *12*, 30.
668 Kawaguchi, Y., Wilson, C.J., and Emson, P.C. (1990). Projection subtypes of rat neostriatal matrix
669 cells revealed by intracellular injection of biocytin. The Journal of neuroscience : the official journal
670 of the Society for Neuroscience *10*, 3421-3438.
671 Kim, H.F., Amita, H., and Hikosaka, O. (2017). Indirect Pathway of Caudal Basal Ganglia for
672 Rejection of Valueless Visual Objects. Neuron *94*, 920-930 e923.
673 Kim, H.F., Ghazizadeh, A., and Hikosaka, O. (2014). Separate groups of dopamine neurons innervate
674 caudate head and tail encoding flexible and stable value memories. Frontiers in neuroanatomy *8*, 120.
675 Kim, H.F., and Hikosaka, O. (2013). Distinct basal ganglia circuits controlling behaviors guided by
676 flexible and stable values. Neuron *79*, 1001-1010.
677 Kim, H.F., and Hikosaka, O. (2015). Parallel basal ganglia circuits for voluntary and automatic
678 behaviour to reach rewards. Brain : a journal of neurology *138*, 1776-1800.
679 Kohno, J., Shiosaka, S., Shinoda, K., Inagaki, S., and Tohyama, M. (1984). Two distinct strio-nigral
680 substance P pathways in the rat: An experimental immunohistochemical study. Brain research *308*,
681 309-317.
682 Krajeski, R.N., Macey-Dare, A., van Heusden, F., Ebrahimjee, F., and Ellender, T.J. (2019).
683 Dynamic postnatal development of the cellular and circuit properties of striatal D1 and D2 spiny
684 projection neurons. The Journal of physiology *597*, 5265-5293.
685 Kreitzer, A.C., and Malenka, R.C. (2008). Striatal plasticity and basal ganglia circuit function.
686 Neuron *60*, 543-554.
687 Kuramoto, E., Furuta, T., Nakamura, K.C., Unzai, T., Hioki, H., and Kaneko, T. (2009). Two types
688 of thalamocortical projections from the motor thalamic nuclei of the rat: a single neuron-tracing study
689 using viral vectors. Cerebral cortex *19*, 2065-2077.
690 Lança, A.J., Boyd, S., Kolb, B.E., and Van Der Kooy, D. (1986). The development of a Patchy
691 organization of the rat striatum. Developmental Brain Research *27*, 1-10.
692 Levesque, M., and Parent, A. (2005). The striatofugal fiber system in primates: a reevaluation of its
693 organization based on single-axon tracing studies. Proceedings of the National Academy of Sciences
694 of the United States of America *102*, 11888-11893.
695 Ma, Y., Hioki, H., Konno, M., Pan, S., Nakamura, H., Nakamura, K.C., Furuta, T., Li, J.L., and
696 Kaneko, T. (2011). Expression of gap junction protein connexin36 in multiple subtypes of
697 GABAergic neurons in adult rat somatosensory cortex. Cerebral cortex *21*, 2639-2649.
698 Menegas, W., Akiti, K., Amo, R., Uchida, N., and Watabe-Uchida, M. (2018). Dopamine neurons
699 projecting to the posterior striatum reinforce avoidance of threatening stimuli. Nature neuroscience
700 *21*, 1421-1430.
701 Menegas, W., Babayan, B.M., Uchida, N., and Watabe-Uchida, M. (2017). Opposite initialization to
702 novel cues in dopamine signaling in ventral and posterior striatum in mice. eLife *6*.
703 Menegas, W., Bergan, J.F., Ogawa, S.K., Isogai, Y., Umadevi Venkataraju, K., Osten, P., Uchida, N.,
704 and Watabe-Uchida, M. (2015). Dopamine neurons projecting to the posterior striatum form an
705 anatomically distinct subclass. eLife *4*, e10032.

Miyamoto, Y., Katayama, S., Shigematsu, N., Nishi, A., and Fukuda, T. (2018). Striosome-based map of the mouse striatum that is conformable to both cortical afferent topography and uneven distributions of dopamine D1 and D2 receptor-expressing cells. Brain structure & function.

Miyamoto, Y., Nagayoshi, I., Nishi, A., and Fukuda, T. (2019). Three divisions of the mouse caudal striatum differ in the proportions of dopamine D1 and D2 receptor-expressing cells, distribution of dopaminergic axons, and composition of cholinergic and GABAergic interneurons. Brain structure & function *224*, 2703-2716.

Moriizumi, T., Leduc-Cross, B., Wu, J.Y., and Hattori, T. (1992). Separate neuronal populations of the rat substantia nigra pars lateralis with distinct projection sites and transmitter phenotypes. Neuroscience *46*, 711-720.

Mowery, T.M., Penikis, K.B., Young, S.K., Ferrer, C.E., Kotak, V.C., and Sanes, D.H. (2017). The Sensory Striatum Is Permanently Impaired by Transient Developmental Deprivation. Cell reports *19*, 2462-2468.

Nambu, A. (2008). Seven problems on the basal ganglia. Current opinion in neurobiology *18*, 595-604.

Ogata , K., Karube, F., Hirai, Y., Fuyjiyama, F. (2018) The unique distribution of D1 and D2 dopamine receptors in the lateral caudal striatum of rodents. Annual Meeting of Society for Neuroscience 2018. Abstract number 146.14. In San Diego, November 3-7.

Paxinos, G., and Franklin, K.B. (2013). The mouse brain in stereotaxic coordinates., 4th edn (Amsterdam: Elsevier).

Peak, J., Hart, G., and Balleine, B.W. (2019). From learning to action: the integration of dorsal striatal input and output pathways in instrumental conditioning. The European journal of neuroscience *49*, 658-671.

Poulin, J.F., Caronia, G., Hofer, C., Cui, Q., Helm, B., Ramakrishnan, C., Chan, C.S., Dombeck, D.A., Deisseroth, K., and Awatramani, R. (2018). Mapping projections of molecularly defined dopamine neuron subtypes using intersectional genetic approaches. Nature neuroscience *21*, 1260-1271.

Redgrave, P., Vautrelle, N., and Reynolds, J.N. (2011). Functional properties of the basal ganglia's re-entrant loop architecture: selection and reinforcement. Neuroscience *198*, 138-151.

Rosen, G. D. and R. W. Williams (2001). Complex trait analysis of the mouse striatum: independent QTLs modulate volume and neuron number. BMC Neurosci *2*: 5.

Saint-Cyr, J.A., Ungerleider, L.G., and Desimone, R. (1990). Organization of visual cortical inputs to the striatum and subsequent outputs to the pallido-nigral complex in the monkey. The Journal of comparative neurology *298*, 129-156.

Selemon, L.D., and Goldman-Rakic, P.S. (1990). Topographic intermingling of striatonigral and striatopallidal neurons in the rhesus monkey. The Journal of comparative neurology *297*, 359-376.

Shepherd, G.M. (2013). Corticostriatal connectivity and its role in disease. Nature reviews Neuroscience *14*, 278-291.

Shipp, S. (2016). The functional logic of corticostriatal connections. Brain structure & function.

Sonntag, M., Englitz, B., Kopp-Scheinpflug, C., and Rubsamen, R. (2009). Early postnatal development of spontaneous and acoustically evoked discharge activity of principal cells of the medial nucleus of the trapezoid body: an in vivo study in mice. The Journal of neuroscience : the official journal of the Society for Neuroscience *29*, 9510-9520.

Takada, M. (1992). The lateroposterior thalamic nucleus and substantia nigra pars lateralis: Origin of dual innervation over the visual system and basal ganglia. Neuroscience letters *139*, 153-156.

751 Tinterri, A., Menardy, F., Diana, M.A., Lokmane, L., Keita, M., Coulpier, F., Lemoine, S., Mailhes,
752 C., Mathieu, B., Merchan-Sala, P., *et al.* (2018). Active intermixing of indirect and direct neurons
753 builds the striatal mosaic. Nature communications *9*, 4725.
754 Valjent, E., and Gangarossa, G. (2021). The Tail of the Striatum: From Anatomy to Connectivity and
755 Function. Trends in neurosciences *44*, 203-214.
756 Watabe-Uchida, M., Zhu, L., Ogawa, S.K., Vamanrao, A., and Uchida, N. (2012). Whole-brain
757 mapping of direct inputs to midbrain dopamine neurons. Neuron *74*, 858-873.
758 Xiong, Q., Znamenskiy, P., and Zador, A.M. (2015). Selective corticostriatal plasticity during
759 acquisition of an auditory discrimination task. Nature *521*, 348-351.
760 Yamamoto, S., Monosov, I.E., Yasuda, M., and Hikosaka, O. (2012). What and where information in
761 the caudate tail guides saccades to visual objects. The Journal of neuroscience : the official journal of
762 the Society for Neuroscience *32*, 11005-11016.
763 Yasuda, M., and Hikosaka, O. (2015). Functional territories in primate substantia nigra pars reticulata
764 separately signaling stable and flexible values. Journal of neurophysiology *113*, 1681-1696.
765 Yasui, Y., Nakano, K., Kayahara, T., and Mizuno, N. (1991). Non-dopaminergic projections from the
766 substantia nigra pars lateralis to the inferior colliculus in the rat. Brain research *559*, 139-144.
767 Yeterian, E.H., and Pandya, D.N. (1998). Corticostriatal connections of the superior temporal region
768 in rhesus monkeys. The Journal of comparative neurology *399*, 384-402.
769 Yeterian, E.H., and Van Hoesen, G.W. (1978). Cortico-striate projections in the rhesus monkey: The
770 organization of certain cortico-caudate connections. Brain research *139*, 43-63.
771 Zheng, Q.Y., Johnson, K.R., and Erway, L.C. (1999). Assessment of hearing in 80 inbred strains of
772 mice by ABR threshold analyses. Hearing research *130*, 94-107.

773

774

10 Tables

Table 1 Primary antibodies used in this study

Antigen	Host species	dilution	Supplier catalogue #	RRID
Alexa 488	rabbit	1:2,000	Thermo Fisher Scientific A10094	AB_221544
DARPP32	goat	1:500	Frontier Institute DARPP-Go-A1090	AB_2571684
dopamine receptor D1	guinea pig	1:500	Frontier Institute D1R-GP-Af500	AB_2571595
dopamine receptor D1	rat	1:500	Sigma Aldrich D2944	AB_10466396
dopamine receptor D2	guinea pig	1:500	Frontier Institute D2R-GP-Af500	AB_2571597
dopamine receptor D2	rabbit	1:500	Frontier Institute D2R-Rb-Af960	AB_2571596
dopamine transporter	goat	1:1,000	Frontier Institute DAT-Go-Af980	AB_2571687
NeuN	mouse	1:10,000	Millipore MAB377	AB_10048713
NeuN	rabbit	1:1,000	Millipore ABN78	AB_10807945

parvalbumin	guinea pig	1:4,000	Synaptic Systems 195004	AB_2156476
Phaseolus Vulgaris Agglutinin (E+L)	goat	1:1,000	Vector AS-2224-1	AB_10000080
tyrosine hydroxylase	mouse	1:2,000	Millipore MAB318	AB_2313764

777

778 **Table 2. Secondary antibodies used in this study.**

antibody	Host species	dilution	Supplier catalogue #	RRID
Anti-goat Alexa Fluor 546	donkey	1:500	Thermo Fisher Scientific A11056	AB_10584485
Anti-goat Alexa Fluor 633	donkey	1:500	Thermo Fisher Scientific A21082	AB_2535739
Anti-guinea pig Alexa Fluor 488	donkey	1:500	Jackson Immunoresearch 706-545-148	AB_2341098
Anti-guinea pig Alexa Fluor 555	goat	1:500	Thermo Fisher Scientific A21435	AB_2535856
Anti-guinea pig Alexa Fluor 633	goat	1:500	Thermo Fisher Scientific A21105	AB_2535757
Anti-mouse Alexa Fluor 488	donkey	1:500	Thermo Fisher Scientific A21202	AB_2535788
Anti-mouse Alexa Fluor 546	donkey	1:500	Thermo Fisher Scientific A10036	AB_2534012
Anti-mouse Alexa Fluor 635	goat	1:500	Thermo Fisher Scientific A31575	AB_2536185

Anti-rabbit-biotin-SP	donkey	1:100	Jackson Immunoresearch #711-065-152	AB_2340593
Anti-rabbit Alexa Fluor 488	donkey	1:500	Thermo Fisher Scientific A21206	AB_2535792
Anti-rabbit Alexa Fluor 546	donkey	1:500	Thermo Fisher Scientific A10040	AB_2534016
Anti-rabbit Alexa Fluor 635	goat	1:500	Thermo Fisher Scientific A31577	AB_2536187

779

780

781 **Table 3. Electrophysiological properties of DARPP32 positive neurons in the dorsal striatum,**

782 **D1R or D2R poor zones.**

	caudo-dorsal striatum	D1R-poor zone	D2R-poor zone	*p* value
resting membrane potential (mV)	-81.1 ± 2.4	-78.1 ± 3.0	-78.6 ± 4.18	0.23
input resistance (MΩ)	52.7 ± 8.6	77.4 ± 20.0	85.3 ± 36.4	0.07
time constant (ms)	4.33 ± 1.7	6.0 ± 2.1	6.7 ± 1.94	0.197
action potential width (ms)	1.57 ± 0.1	1.60 ± 0.44	1.56 ± 0.25	0.98
max action potential frequency (Hz)	25.0 ± 13.2	34.2 ± 11.4	34.0 ± 8.0	0.42
number of neurons	6	5	3	

783

784

785

786

787

788

789

11 Figure Legends

Figure 1. Uneven distribution of dopamine receptor D1 (D1R), dopamine receptor D2 (D2R), and tyrosine hydroxylase (TH) in the caudal striatum.

(A) Immunofluorescent images against D1R (magenta), D2R (green), and TH (cyan) of the mouse striatum. Arrowheads indicate the regions with very faint signal as either D1R or D2R. In this paper, the lateral striatum is subdivided into the rostral (rStr) and caudal striatum (cStr); the dorsal (dStr) and ventral striatum (vStr); cStr is further divided into the caudo-dorsal (cdStr) and caudoventral striatum (cvStr), as shown in the rightmost panel. cvStr contains D1R- and D2R-poor zones. The region surrounding the poor zones is named here as para-poor zone in which D1R and D2R express nearly uniformly. (B) Quantification of pixel intensity along with a dotted white line. Gray bar presents the rostral and caudal edges of the striatum. The right panel shows normalized pixel intensity in a section of a mouse (3.0 mm lateral from the midline). (C) Average pixel intensity (N = 3 mice). Circles indicate individual data. AST, amygdala striatal transition area; Cx, cerebral cortex; ic, internal capsule; v, ventricle. ***$p < 0.001$.

Figure 2. Uneven distribution of dopamine receptor D1 (D1R) or dopamine receptor D2 (D2R) mRNA expressing neurons in the caudal striatum.

(A), (D) Left, Immunofluorescent images against D1R (green) and D2R (magenta). Right, Drd1a- (A) or Drd2- (D) expressing neurons (blue) with immunostaining against NeuN (brown). (B), (E) Magnified images of rectangle areas 1-4 in A or D. (C), (F) Proportion of Drd1a- or Drd2-expressing neurons in rostral (rStr), para-poor zone (ppz), D1R-poor zone (D1p) or D2R-poor zone (D2p). (N = 3 mice for each) (G) Mean NeuN+ cell number in each ROI. (H) Elucidated cell composition in each striatal area. AST, amygdala striatal transition area; Cx, cerebral cortex; ic, internal capsule; v, ventricle. **$p < 0.01$.

Figure 3. Whole cell recording from the caudal striatum.

(A), An example of the whole cell recorded neurons. The location of the recorded neurons was confirmed using post-hoc immunofluorescence for dopamine receptor D1 (D1R) (magenta) and dopamine receptor D2 (D2R) (green). Recorded neurons are shown in cyan. The left neuron (arrow) is situated in D2R-poor zone, whereas the dendrites of the right neuron (arrowhead) are in D1R-poor zone. The cell body of the right neurons was not confined in this section. (B) A magnified image of the left neuron in A. Left, note many spines protruded from the dendrites. Inset shows further magnified view of the dotted rectangle area. Right, the neuron (asterisk) expressed DARPP32, a marker of MSNs. (C) Representative traces of membrane voltages responding to depolarized (100 and 500 pA) and hyperpolarized (-100 pA) current pulses. MSNs in the caudo-dorsal striatum (top), D1R-poor zone (middle), and D2R-poor zone (bottom) possessed similar membrane properties (see also Table 3).

Figure 4. Uneven distribution of direct pathway neurons in the caudal striatum.

(A) Retrograde labeling of the direct pathway neurons using bulk injection of CTB 555 in substantia nigra. Note the bulk injection spread broadly; however, globus pallidus (GP), the target of the indirect pathway, is not invaded. (B) Retrogradely labeled striatal direct pathway neurons are distributed throughout the striatum, except the dopamine receptor D1 (D1R)-poor zone (D1p). (C) Magnified images of retrogradely labeled neurons in the rostral striatum, caudal striatum, D1R-poor zone, and dopamine receptor D2 (D2R)-poor zone. The locations of them were indicated in the leftmost panel as rectangles 1-4. (D) Density of retrogradely-labeled neurons in each subregion. D1R-poor zone contained significantly small number of labeled neurons than the other subregions, whereas larger number of labeled neurons existed in D2R-poor zone. * $p < 0.05$; ** $p < 0.01$. (E) Detection of Drd1a or Drd2 mRNA expression using *in situ* hybridization (blue) combined with immunohistochemistry against CTB (brown; arrowheads). Note CTB-labeled neurons expressed Drd1a (E) but not Drd2 (F).

Figure 5. Anterograde axon tracing of the caudal striatum.

(A) An example of biotinylated dextran amine (BDA) injection. The injection site was located in the dopamine receptor D1 (D1R)-poor zone. (B) Labeled axons from D1R-poor zone in GP, EP, and internal capsule (ic). Left, BDA labeled axons. Right, NeuN staining. (C) A magnified image of EP. Faint BDA labeling was observed in EP (arrowheads). More bright axons existed outside of EP (arrows). (D) Left, Dense BDA labeled axons in SNpl. Right, A magnified image of SNpl. Note axons were located in SNpl, where tyrosine hydroxylase (TH)-expressing neurons (magenta) did not exist. (E) Phaseolus Vulgaris Leucoagglutinin (PHAL) injection to the dorsal part of caudal Str (cdStr), not containing D1R- or dopamine receptor D2 (D2R)-poor zone. (F) cdStr also projected to SNpl, being relatively dense in the ventral part of SNpl. Amy, amygdala; Cx, cerebral cortex; EP, entopeduncular nucleus; GP, globus pallidus; ic, internal capsule; Str, striatum; SNpc, substantia nigra pars compacta; SNpl, substantia nigra pars lateralis; SNpr, substantia nigra pars reticulata.

Figure 6. The indirect pathway from caudal striatum (cStr).

(A) Biotinylated dextran amine (BDA) injection to poor zones labeled axons in the caudal globus pallidus (GP), but only few axons in the rostral GP (arrowheads). Arrow indicates descending axons toward the downstream nuclei. The images were arranged from rostral (the upper left) to caudal (the lower right). (B) Retrograde tracer, fluorogold, injection to SNpl visualized both cStr neurons and GP neurons. Dopamine receptor D1 (D1R)- and dopamine receptor D2 (D2R)-poor zones were confirmed using immunofluorescence. A rectangle area shown in B was magnified in C. (C) Neurons projecting to SNpl were frequently located in D2R-poor zone (D2p) than in D1R-poor zone (D1p). Note GP neurons were also frequently labeled in the caudal GP. (D) Fluorogold injection to SNpl, counter stained with calbindin-D-28k (top). Fluorogold extended to the lateral part of SNpr. PBP,

parabrachial pigmented nucleus; SNpl, substantia nigra pars lateralis; SubG, superficial gray layer of the superior colliculus; VTA, ventral tegmental area.

Figure 7. Uneven distribution of dopamine receptor D1 (D1R), dopamine receptor D2 (D2R), and tyrosine hydroxylase (TH) in the caudal striatum existed in mice, rats, and common marmosets.

(A)-(D) Immunofluorescent images against D1R (green), D2R (magenta), and TH (cyan) in the striatum of rodents. Arrowheads indicate D1R- or D2R-poor zone (D1p or D2p). The distance from the midline was shown at the lower left corner of the upper panels. (E) Uneven distribution in the caudate of marmosets. (F) A magnified view of the CDt, including the poor zones. AST, amygdala striatal transition area; CDh, caudate head; CDt, caudate tail; Cx, cerebral cortex; ic, internal capsule; v, ventricle.

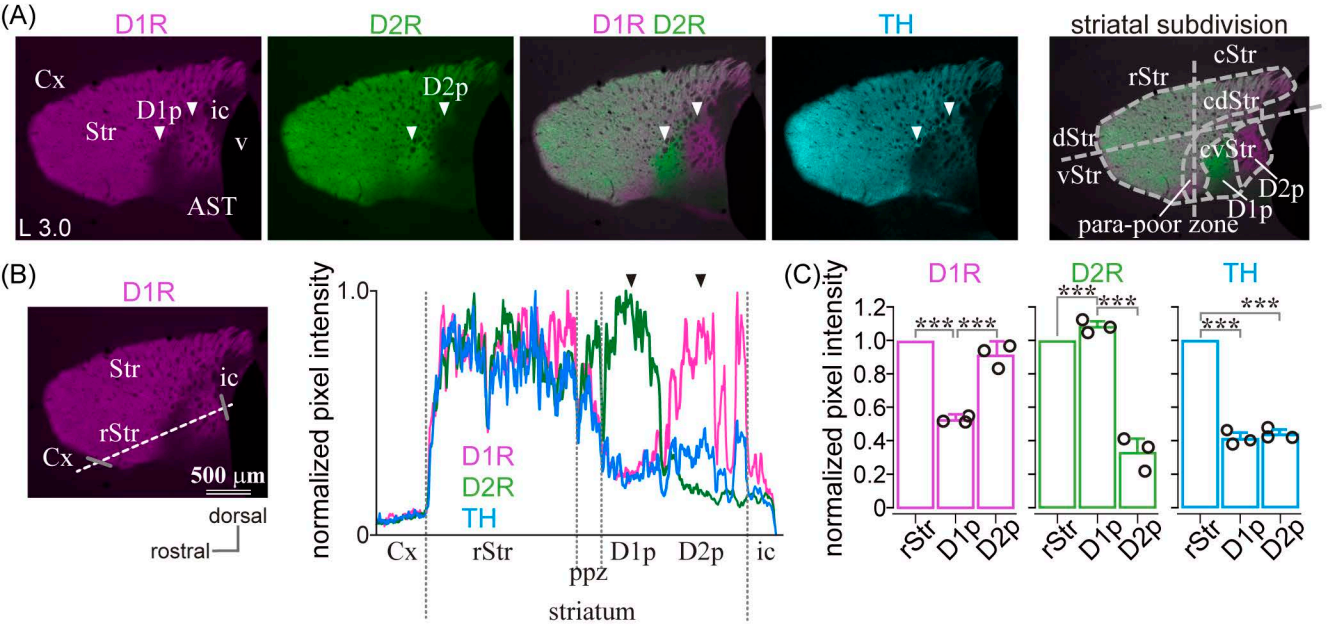
(A)
D1R
D2R
D1R D2R
TH
striatal subdivision
Cx
Str
D1p
ic
v
AST
L 3.0
D2p
rStr
cStr
cdStr
dStr
cvStr
vStr
D2p
D1p
para-poor zone
(B)
D1R
Str
ic
rStr
Cx
500 μm
dorsal
rostral
normalized pixel intensity
1.0
0
D1R
D2R
TH
Cx
rStr
ppz
D1p
D2p
ic
striatum
(C)
D1R
D2R
TH
normalized pixel intensity
1.2
1.0
0.8
0.6
0.4
0.2
0
***
rStr
D1p
D2p

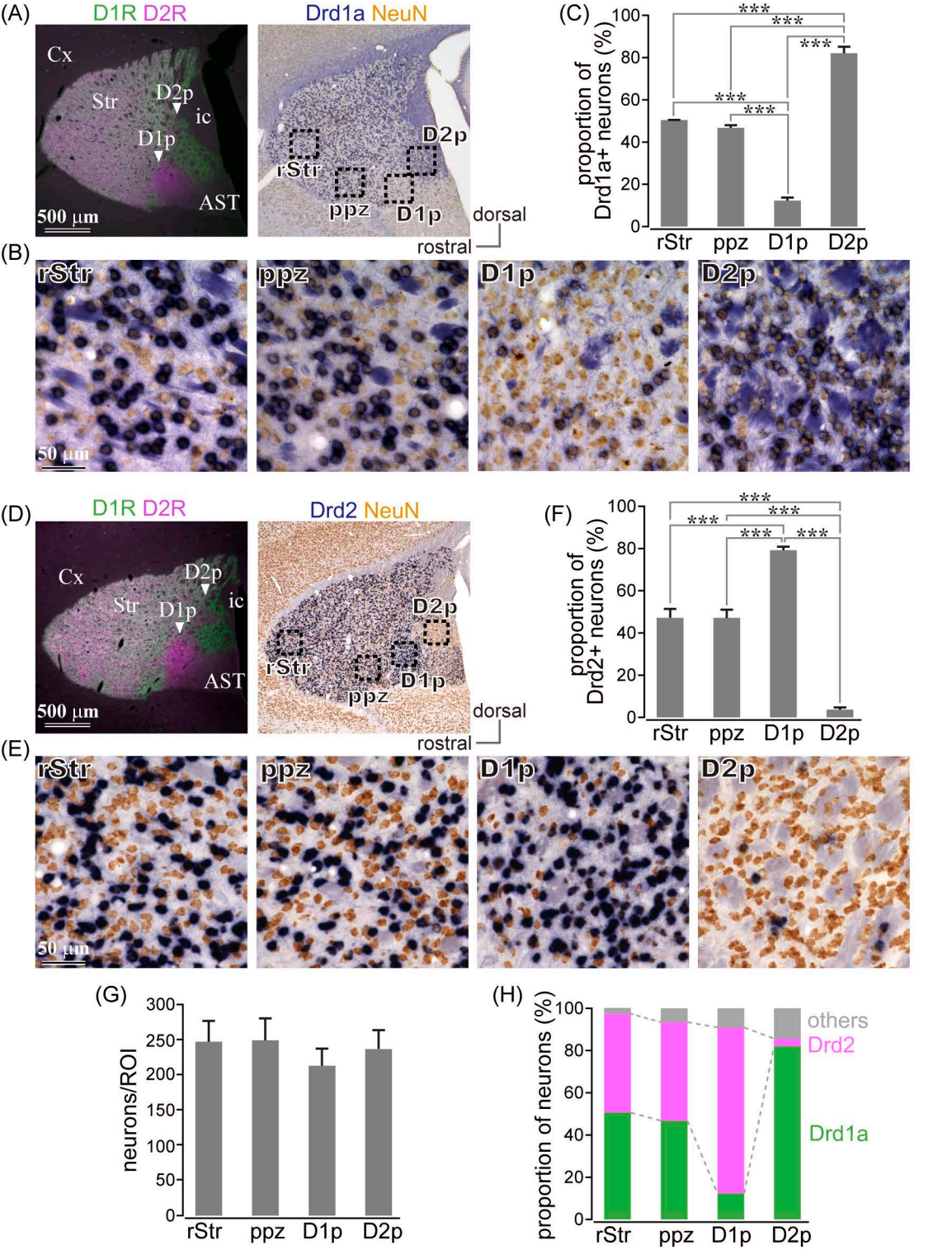
(A)
D1R D2R
Cx
Str
D2p
ic
D1p
AST
500 μm
Drd1a NeuN
rStr
ppz
D1p
D2p
dorsal
rostral
(B)
rStr
ppz
D1p
D2p
50 μm
(C)
proportion of Drd1a+ neurons (%)
***
rStr
ppz
D1p
D2p
(D)
D1R D2R
Drd2 NeuN
(E)
(F)
proportion of Drd2+ neurons (%)
(G)
neurons/ROI
(H)
proportion of neurons (%)
others
Drd2
Drd1a

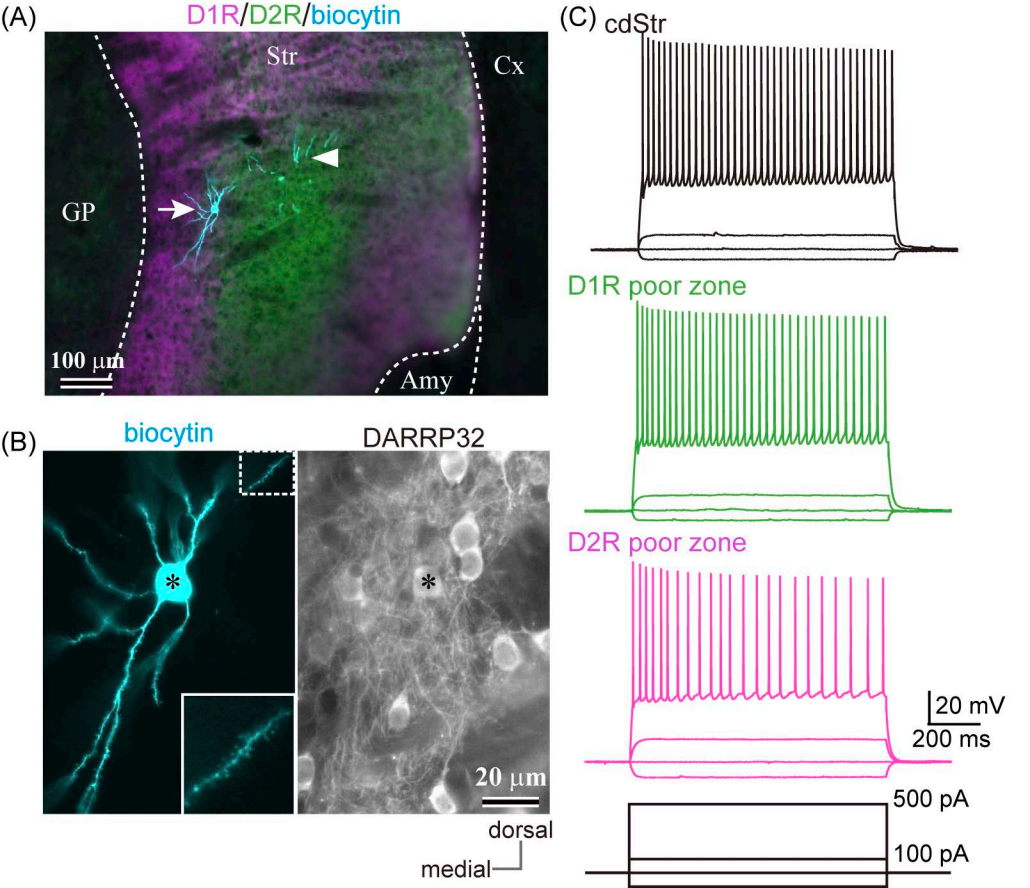
(A)
D1R/D2R/biocytin
Str
Cx
GP
100 μm
Amy
(B)
biocytin
DARRP32
20 μm
dorsal
medial
(C) cdStr
D1R poor zone
D2R poor zone
20 mV
200 ms
500 pA
100 pA

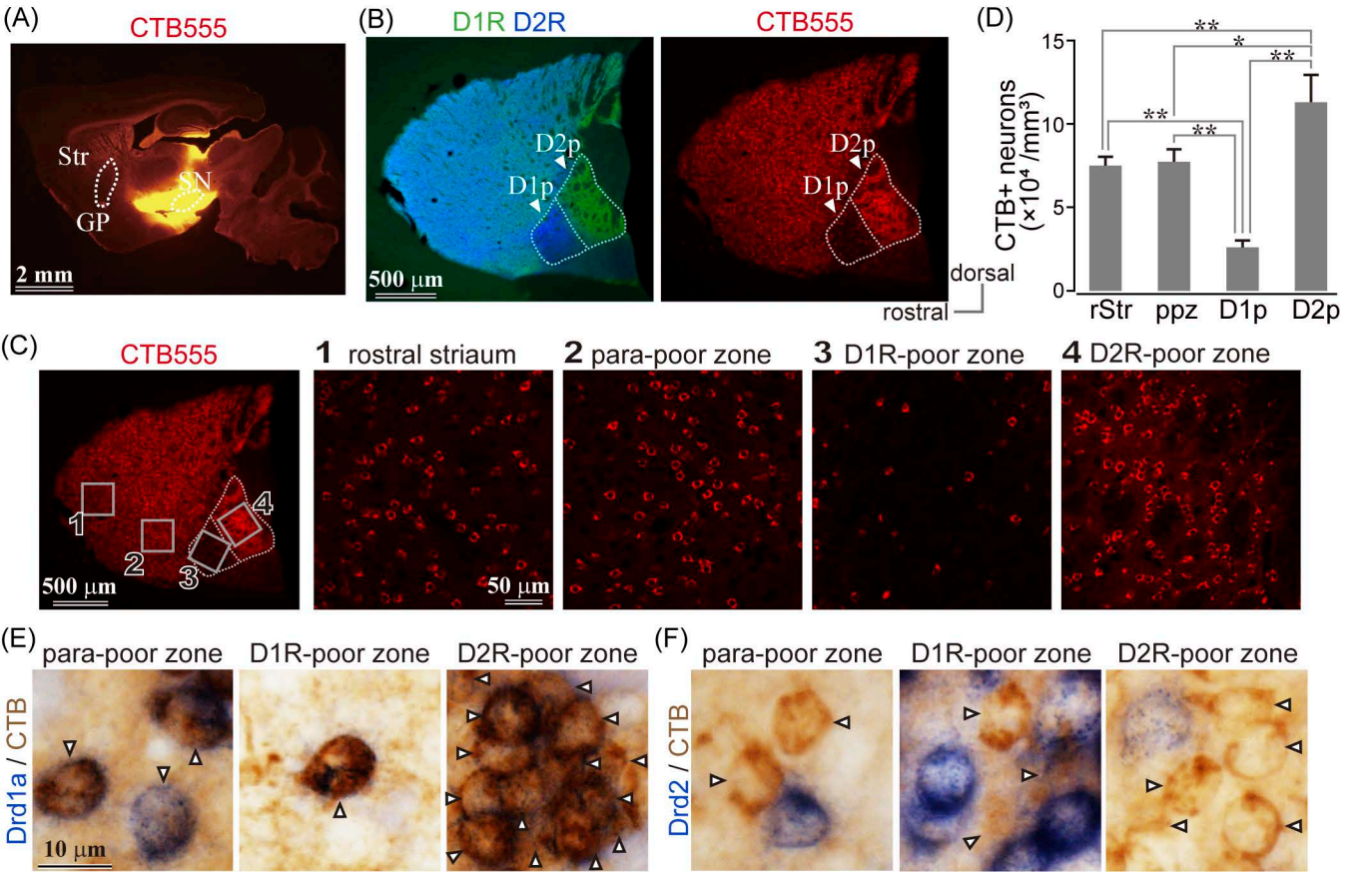
(A)
CTB555
Str
SN
GP
2 mm
(B)
D1R D2R
CTB555
D2p
D1p
500 μm
dorsal
rostral
(D)
CTB+ neurons
(×10⁴ /mm³)
15
10
5
0
**
*
**
**
**
rStr
ppz
D1p
D2p
(C)
CTB555
1 rostral striaum
2 para-poor zone
3 D1R-poor zone
4 D2R-poor zone
500 μm
50 μm
(E)
para-poor zone
D1R-poor zone
D2R-poor zone
Drd1a / CTB
10 μm
(F)
para-poor zone
D1R-poor zone
D2R-poor zone
Drd2 / CTB

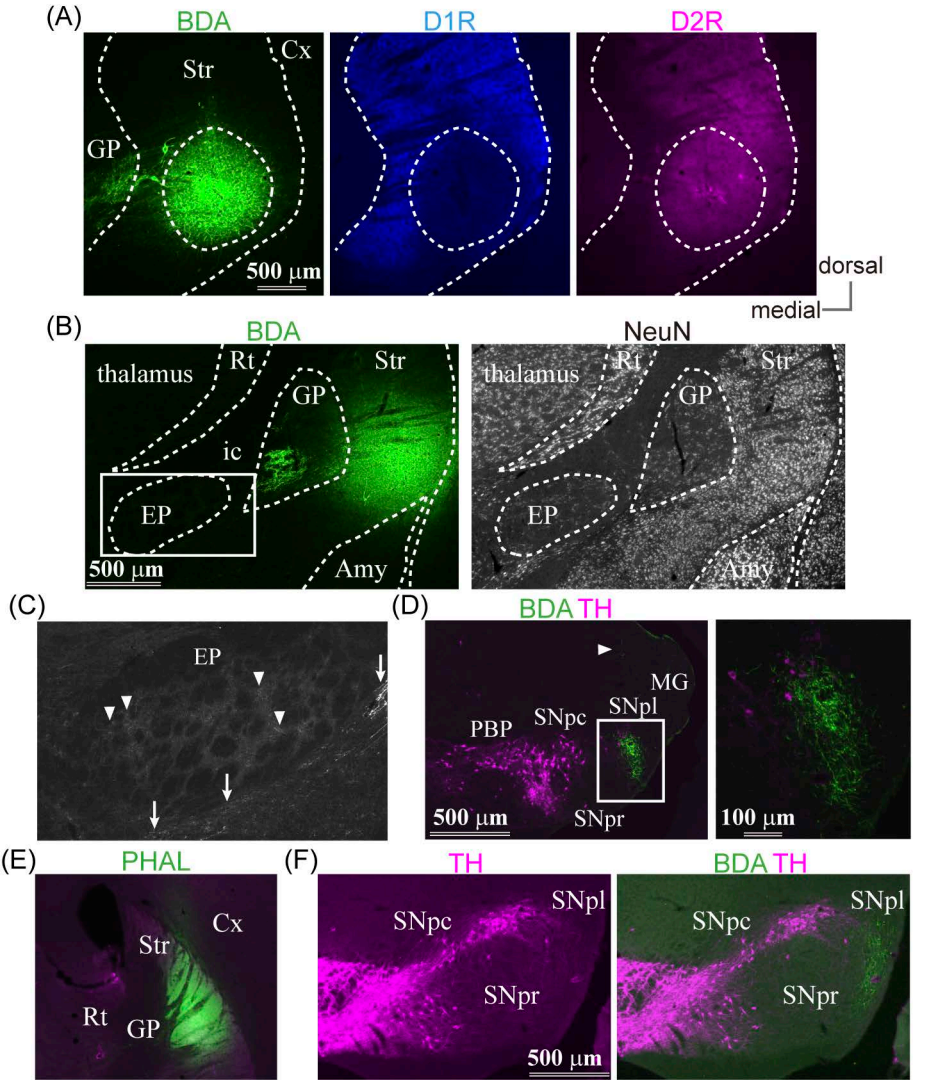
(A)
BDA
D1R
D2R
Str
Cx
GP
500 μm
dorsal
medial
(B)
BDA
NeuN
thalamus
Rt
Str
GP
ic
EP
Amy
500 μm
(C)
EP
(D)
BDA TH
MG
SNpl
PBP
SNpc
SNpr
500 μm
100 μm
(E)
PHAL
Cx
Str
Rt
GP
(F)
TH
BDA TH
SNpl
SNpc
SNpr
500 μm

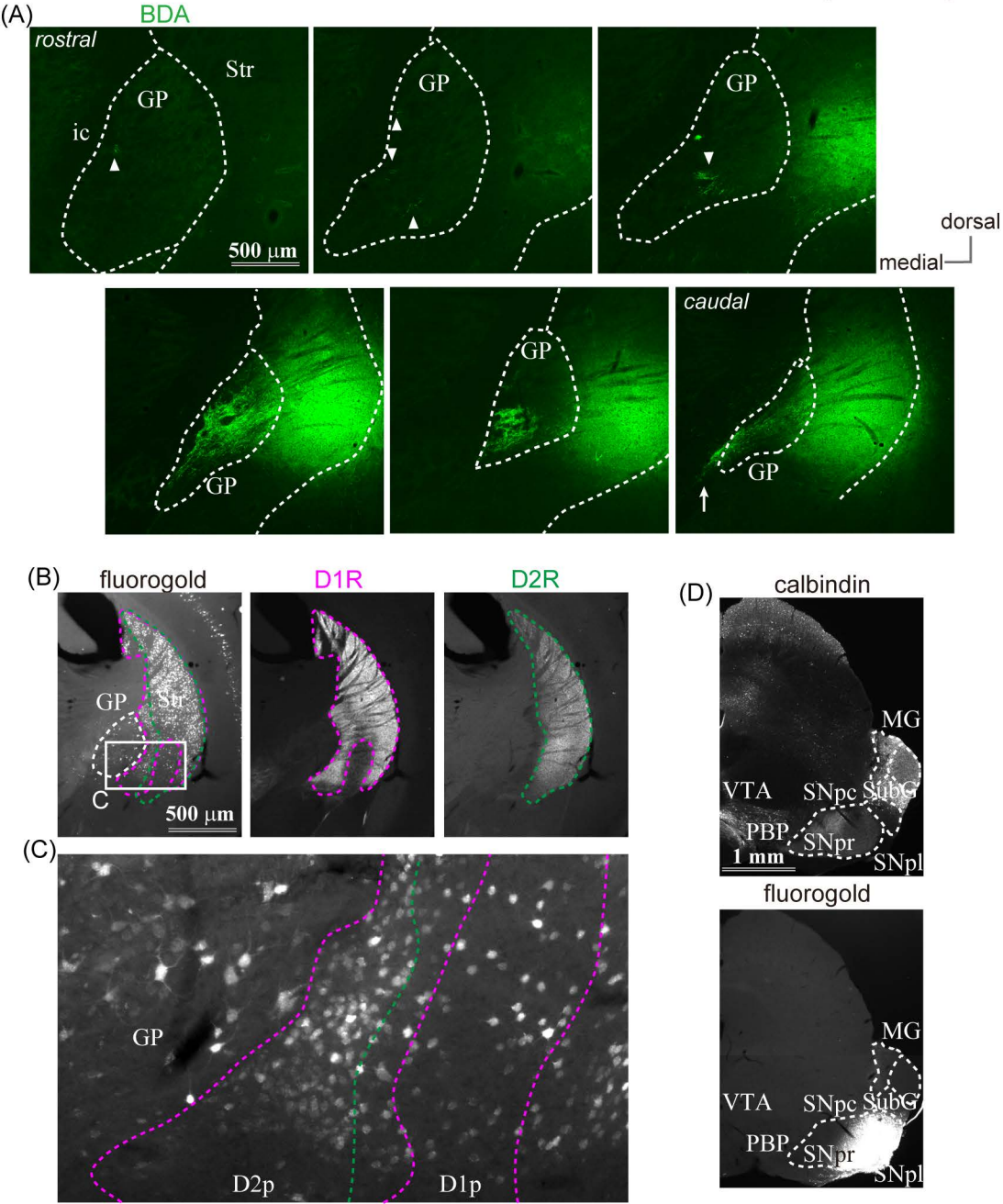
(A)
BDA
rostral
Str
GP
ic
500 μm
GP
GP
dorsal
medial
GP
GP
caudal
GP
(B)
fluorogold
D1R
D2R
GP
Str
C
500 μm
(C)
GP
D2p
D1p
(D)
calbindin
MG
VTA
SNpc
SubG
PBP
SNpr
1 mm
SNpl
fluorogold
MG
VTA
SNpc
SubG
PBP
SNpr
SNpl

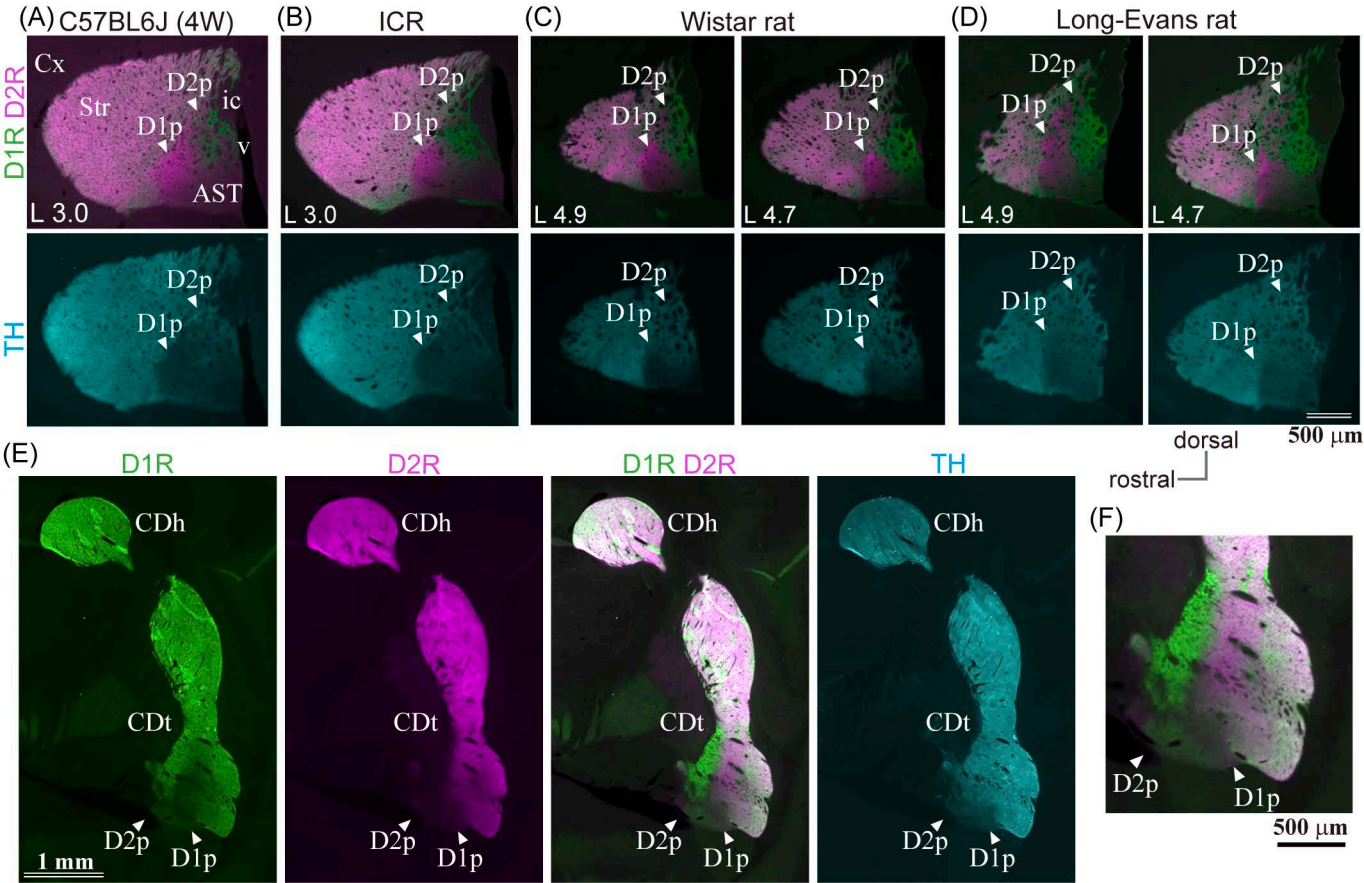
(A) C57BL6J (4W)
(B) ICR
(C) Wistar rat
(D) Long-Evans rat
D1R D2R
TH
Cx
Str
ic
v
AST
D2p
D1p
L 3.0
L 4.9
L 4.7
500 μm
(E)
D1R
D2R
D1R D2R
TH
CDh
CDt
1 mm
dorsal
rostral
(F)